Electrochimica Acta 426 (2022) 140790

Contents lists available at ScienceDirect

Electrochimica Acta

journal homepage: www.journals.elsevier.com/electrochimica-acta

A promising silicon/carbon xerogel composite for high-rate and high-capacity lithium-ion batteries

Lucía dos Santos-Gómez [a,*], Nuria Cuesta [b], Ignacio Cameán [c,*], S. García-Granda [a], Ana B. García [c], Ana Arenillas [c]

[a] Department of Physical and Analytical Chemistry, University of Oviedo – CINN-CSIC, Avda. Julián Clavería 8, Campus de El Cristo, Oviedo 33006, Spain
[b] Nanomaterials and Nanotechnology Research Center, CINN-CSIC, El Entrego, Asturias 33940, Spain
[c] Instituto de Ciencia y Tecnología del Carbono, INCAR-CSIC, Francisco Pintado Fe 26, Oviedo 33011, Spain

ARTICLE INFO

Keywords:
Silicon
Carbon xerogel
Si/C composite
Anode
Lithium-ion battery

ABSTRACT

Silicon-based anodes are widely studied as an alternative to graphite anodes for lithium-ion batteries. Nevertheless, their practical application is mainly limited by the huge volume change that silicon particles undergo due to alloying and de-alloying with lithium ions during discharge/charge processes, which result in cracks and electrode degradation. In the present study, porous silicon-carbon composites are investigated as anode materials for next-generation lithium-ion batteries. These composites are prepared by a cost-effective, easily-scalable method based on a microwave assisted approach for the carbon matrix, followed by dispersion of the silicon in 2-propanol. The electrochemical behavior of the Si/C composites with different proportions of silicon is evaluated in terms of alloying and de-alloying mechanisms of lithium ions, battery reversible capacity, irreversible capacity in the first cycle, retention of capacity along cycling, and cycle efficiency. The composite with 30 wt.% of silicon presents specific discharge capacity as high as 917 mAh g^{-1} after 200 cycles and excellent stability in the long-term at high current density, which makes it a promising candidate for the lithium-ion battery market.

1. Introduction

Lithium-ion batteries (LIBs) are among the most favorable energy storage devices on the market due to their long cycling performance, high energy density, and low self-discharge [1–3]. Nevertheless, the power density that current batteries can provide is limited to 100–300 W kg^{-1} and they need long charging times. Novel anode materials with high capacity lithium storage and high stability are crucial for improving the charging rate, battery life and specific energy.

Generally, graphite has been widely used as an anode material because of its low cost, good electrical conductivity, low working voltage, and high coulombic efficiency (> 95%) [1–3]. However, graphite has a limited theoretical capacity of 372 mAh g^{-1} and suffers from the generation of lithium dendrites. In this context, various carbon materials have been investigated as anodes for LIBs [4–6]. Among these materials, carbon xerogels have attracted attention for this application because their chemical, structural, and morphological properties can be tailored [7–9]. These xerogels are composed of interconnected nodules which create a three-dimensional framework. Moreover, their pore size distribution can be customized by modifying synthesis conditions [10–12]. Some authors have incorporated highly conductive additives into the xerogel matrix to enhance electron mobility [13–16]. Others have prepared graphitic-type structural ordered carbon xerogels with improved electrical conductivity by microwave heating or by high temperature treatment using a graphene oxide as an additive [17–19], these materials have been investigated as anode materials for LIBs.

Silicon is one of the most promising alternatives for the next generation of LIBs due to its high theoretical capacity (3579 mAh g^{-1}, based on $Li_{15}Si_4$), low working voltage (~ 0.4 V vs. Li/Li^+), abundance, and low environmental impact [20,21]. However, practical application of silicon is limited by many obstacles such as (i) huge volume change variation (~ 360% when $Li_{4.4}Si$ is formed as a final phase) due to alloying and de-alloying with lithium ions during discharge/charge processes, which results in cracks and electrode degradation [22,23]; (ii) low electrical conductivity, which affects electron transmission and thus rate capability [24,25]; and (iii) unstable solid electrolyte interface (SEI), because of repetitive growth due to the continuous cracking and degradation of Si electrodes. Moreover, this

* Corresponding authors.
E-mail addresses: ldsg@uniovi.es (L. Santos-Gómez), icamean@incar.csic.es (I. Cameán).

https://doi.org/10.1016/j.electacta.2022.140790
Received 12 May 2022; Received in revised form 14 June 2022; Accepted 29 June 2022
Available online 1 July 2022

forming-breaking-reforming process consumes lithium ions, increasing SEI thickness and producing severe attenuation of capacity.

Various strategies have been developed to solve these problems, including thin film Si electrodes [26,27], nanostructured electrodes [28–30], porous structures [31], silicon/carbon composites [32–36], alloys with other metals [37], combination with micro- and nano-particles [38], addition of additives [39] and development of more effective binders [40]. Combining silicon with a carbonaceous material seems to be the most effective strategy because, in the resulting silicon/carbon material, silicon acts as the active material and carbon mitigates Si volume changes and enhances conductivity. Recently, several studies on the application of Si/C composites as anodes for LIBs have been reported [41]. However, the high cost due to the complexity of both the synthesis process and the design of the structures makes most of these composite materials unsuitable for industrial production. Therefore, implementation and commercialization of Si/C materials as anodes in LIBs is subject to two factors; the choice of an appropriate carbon material and the development of cost-effective, scalable preparation methods.

In the present study, Si/C composite materials are prepared via an easily-scalable, low-cost approach using a graphitized xerogel (GX) doped with graphene oxide (GO) as a carbon matrix. GX is synthetized by a microwave-assisted synthesis procedure, which is a well-established method for producing carbon xerogels on a large scale, considerably reducing both synthesis cost and time [42]. Subsequently, nano-silicon (nSi) is homogeneously distributed into this matrix by simply preparing a dispersion of the two materials in 2-propanol. The electrochemical performance of the resulting Si/C composites as anodes for next-generation LIBs is investigated by prolonged galvanostatic cycling vs. Li/Li^+ at different current densities. The study examines the influence of the proportion of nSi in the Si/C composite as well as the effect of cycling conditions (voltage range, current density) on electrode reversible capacity, irreversible capacity in the first cycles, retention of capacity along cycling, and cycle efficiency. The alloying and de-alloying mechanism of lithium ions with these novel composites during discharge/charge processes is also discussed.

2. Experimental

2.1. Synthesis of graphitized xerogel doped with graphene oxide

Carbon xerogels doped with graphene oxide were synthesized following the same approach described in the literature [43]. First of all, resorcinol (R) (99 wt.% purity, Indspec) was dissolved in a mixture of distilled water and 85 wt.% of GO aqueous suspension (5 mg/mL, Applynano Solutions S.L.) under constant magnetic stirring. Following that, formaldehyde (F) (37 wt.% aqueous solution, 10–15 wt.% methanol, Ercros) was incorporated to reach an R/F molar ratio of 0.27 and the mixture was stirred until a homogeneous solution was obtained. The dilution ratio (in mol) was determined by dividing the amount of liquid substances (water contained in the formaldehyde solution, methanol contained in the formaldehyde solution and water contained in the GO suspension) by the amount of solids (formaldehyde, resorcinol, and GO). NaOH was used as basification agent to adjust the pH of the solution to 4.74. The resulting solution was heated for 3 h at 85 ºC in a microwave oven to accelerate gelation and the curing process. The doped organic xerogel, thus prepared, was then carbonized for 2 h at 1000 ºC under a 250 mL min^{-1} N_2 flow to obtain the carbon xerogel and to reduce the GO. Finally, the carbonized sample was graphitized by heat treatment at 2800 ºC, in a graphite electric furnace (Xerion Advanced Heating), for 2 h under an Ar flow of 2 L min^{-1}. The graphitized xerogel doped with graphene oxide was labelled as GXGO.

2.2. Preparation of Si/GXGO composites

Si/GXGO composites were prepared by dispersing nanocrystalline silicon powder (97%, Strem Chemicals) and the GXGO in 2-propanol by vigorous mechanical stirring (IKA Overhead Stirrer Eurostar 20) at 70 ºC for 60 min to ensure good homogenization and the absence of agglomerates. The resultant wet dispersion was then dried at 60 ºC for 12 h to evaporate the solvent. This procedure was optimized in a previous work [34]. The total amount of nSi in the composite was 20, 30, 40 and 50 wt. %. Samples without nSi and with 100 wt.% of nSi were also prepared for comparison. Hereafter, composites will be generically designated as YSi/GXGO, where Y indicates the wt.% of nano-silicon.

2.3. Characterization techniques

Materials were characterized by X-ray diffraction (XRD) in a D8 Advance (Bruker) diffractometer with a Göbel mirror configuration. Data was measured from 10 to 75º over a 2θ range with a step size of 0.02º and 3 s per step. The X'Pert HighScore Plus program was used for phase identification [44]. The interplanar distance, d_{002}, and the mean crystallite size along the c axis, L_c, were calculated from the position of the (002) in the corresponding diffractograms by applying Braggs's equation and the Scherrer formula with a value of $K = 0.9$, respectively, as described elsewhere [4].

The meso-macroporous structure of GXGO was calculated by mercury porosimetry (Autopore IV 9500, Micromeritics). N_2 adsorption-desorption isotherms were measured at −196 ºC in a Tristar 3020 instrument (Micromeritics) after outgassing overnight at 120 ºC. Textural parameters such as external surface area (S_{ext}), BET surface area (S_{BET}) and micropore volume (V_{micro}) were determined using the t-plot, Brunauer-Emmett-Teller (BET) and Dubin-Raduskevich (DR) equations, respectively. The total pore volume (V_p) was calculated by the quantity of N_2 adsorbed at the saturation point.

SEM images of the YSi/GXGO composites were obtained with a Quanta FEG 650 microscope employing an Everhart-Thornley secondary electron detector (ETD). The composition was examined by Energy Dispersive X-ray Spectroscopy (EDX) (ametek-EDAX) with an Apollo X detector.

2.4. Electrode preparation, cell assembly and electrochemical measurements

Working electrodes (WEs) containing 70 wt.% of Si/GXGO active material, 20 wt.% of sodium carboxymethylcellulose binder (NaCMC, Sigma-Aldrich, MW ~700,000) and 10 wt.% of carbon black electrical conductive (Super C65, Imerys) were prepared by the following procedure: (i) a solution of 1 wt.% of NaCMC in distilled water was prepared by mechanical stirring in an Overhead Stirrer Eurostar 20 (IKA) at 3000 rpm for 30 min, (ii) the C65 was then added to the NaCMC solution while the stirring continued at 4000 rpm for 10 min to obtain a homogenous dispersion, (iii) the corresponding YSi/GXGO composite was incorporated gently to the dispersion and stirred at 4000 rpm for 1 h to get a uniform slurry without agglomerates, (iv) the slurry was tape-casted at 50 ºC on a copper foil of 25 μm thickness (Goodfellow, > 99.99% purity) using a doctor blade with a 120 μm gap and a monitored/automatic film applicator with a perforated heated vacuum table (Elcometer 4340), (v) the resulting electrode tape was dried in the vacuum table at 80 ºC for 1 h, (vi) subsequently, electrode discs 12 mm in diameter were cut from the tape using a manual punch, and (vii) finally, these electrodes were additionally dried overnight at 120 ºC in vacuum and stored in a glove box (MBraun) under Ar atmosphere, with oxygen and water below 0.1 ppm. The average YSi/GXGO active material mass load in the electrodes was 1 mg cm^{-2}. Working electrodes of GXGO material, a commercial K65 synthetic graphite (SG), supplied from Imerys, and a commercial Si/C composite (carbon coated silicon) with a Si content of 1.92 wt.% (as determined by X-ray Fluorescence Spectrometry, XRF, on the ashes of the material), supplied by Xiamen Tob New Energy Technology Co., Ltd. (TOB-S400A), were also prepared following the same procedures and used in this study for comparative

purposes.

Two-electrode (working and counter) Swagelok-type cells were selected to perform the electrochemical measurements. Metallic lithium (Merck/Sigma Aldrich, 99.9% purity) discs 12 mm in diameter were used as counter electrodes (CE). The electrodes were separated by two micro-fibre glass discs of the same diameter (WHATMAN GF/A) impregnated with 150 μL of the electrolyte, i.e. 1 M $LiPF_6$ salt in a mixture of ethylene carbonate (EC):diethyl carbonate (DEC), 1:1, w:w, with ~1–5 wt.% of vinylene carbonate (VC). The cells were assembled in a glove box (MBraun) under Ar atmosphere and water and oxygen concentration below 0.1 ppm, and their initial potential was in the range of 2.90–3.10 V vs. Li/Li^+. Because in this study the potential always refers to the redox pair Li/Li^+, the term voltage is used instead of potential.

The cells were tested electrochemically to evaluate the performance of the YSi/GXGO composites as anodes for lithium-ion batteries using a biologic multichannel VMP2/Z potentiostat/galvanostat. Prolonged galvanostatic cycling experiments (up to 200 discharge/charge cycles) were carried out in the voltage ranges 2.1–0.003 V and 0.9-X V (X = 0.010, 0.020, 0.040, 0.060 and 0.080 V) at an electrical current density of 1000 mA g^{-1} to determine the optimal low cut-off voltage (LCOV). Once the optimal LCOV was assessed, additional experiments were performed at 100, 500, 1000 and 2000 mA g^{-1} for 200 discharge/charge cycles.

3. Results and discussion

3.1. Structural and textural properties of the graphitized xerogel doped with graphene oxide

Fig. 1 shows the XRD patterns of GXGO, nSi, and 50Si/GXGO composite. GXGO presents two peaks at 2θ of ~ 27° and ~ 54 ° which, respectively, correspond to (002) and (004) reflexions of the graphitic network. There is also a wide peak around 2θ of 43–44 °, which is attributed to the (100) and (101) reflexions. Moreover, the calculated interlayer spacing (d_{002}) of this material is close to that of graphite, i.e. 0.338 nm (GXGO) vs. 0.335 nm (graphite), and its main crystallite size along the c-axis (L_c ~ 12.8 nm) is higher than those determined for carbon xerogels [17]. These results confirm the graphitization of the xerogel, which is favored by the addition of GO to the xerogel precursor solution [18] and the subsequent thermal and mechanical treatment achieves greater uniformity of the graphitic laminates in the composite, as shown in Fig. 1. In previous studies, our group found that the incorporation of GO in the polymeric precursor of the xerogels leads to a considerable change in their structure. This was due to the fact that graphene layers act as seeds, which promote the graphitization process, resulting in a more laminar structure [18]. In the diffractogram of 50Si/GXGO composite, a combination of peaks attributed to GXGO and nSi are clearly visible.

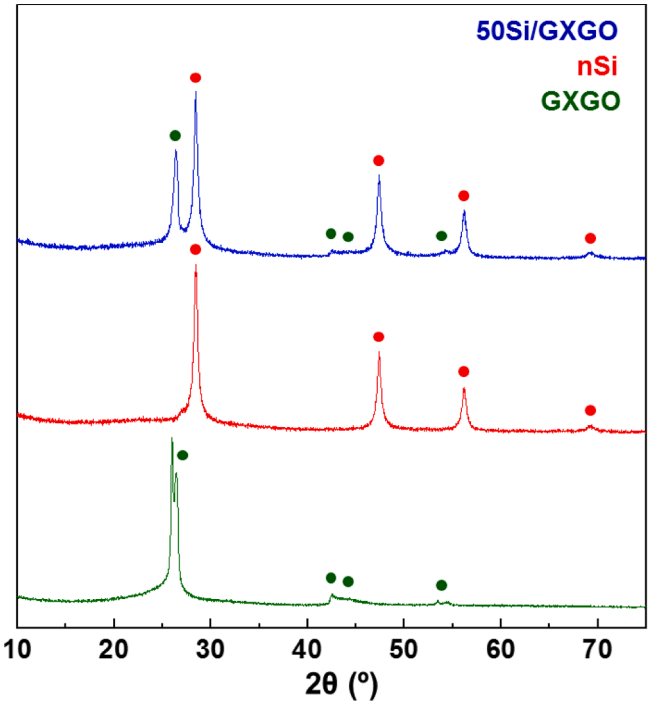

Fig. 1. XRD patterns of GXGO, nSi and 50Si/GXGO composite.

The textural properties of the carbon matrix were studied by N_2 adsorption at −196 °C. Fig. 2a shows the N_2 adsorption-desorption isotherm of GXGO, which is correlated to a reversible type II isotherm (IUPAC classification) of macroporous solids. This isotherm shows a slight increase in N_2 adsorption at low pressures, which reflects a low volume of micropores. This is due to the fact that the graphitization process reorganizes the polymeric structure of the R/F xerogel and produces a collapse of the microporosity [17]. The N_2 adsorbed also increases with pressure and there is a substantive increase at a relative pressure value around 1, which is characteristic of materials with elevated macroporosity. The BET specific surface area is 50 m^2 g^{-1}.

The measurement of pore volumes for macroporous materials by N_2 adsorption is not very accurate. Thus, mercury porosimetry was used to estimate the size and volume of meso- and macropores in the material. The pore size distribution of GXGO is shown in Fig. 2b. The total-, meso-

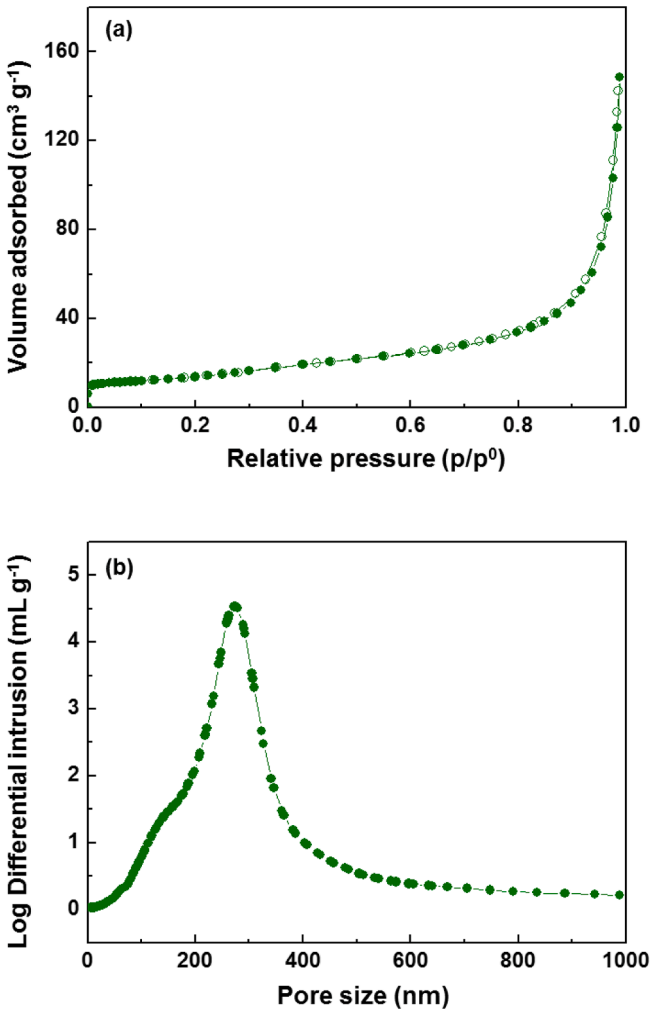

Fig. 2. (a) N_2 adsorption-desorption isotherm and (b) pore size distribution obtained from mercury porosimetry for the GXGO composite.

and macropore volumes are 1.71, 0.05 and 1.66 $cm^3\ g^{-1}$, respectively, and there is a narrow distribution of pore size centred on 275 nm. These results are similar to those for related materials [18].

3.2. Morphology of Si/GXGO composites

The distribution of nSi in the GXGO carbon matrix was examined by SEM/EDX. Fig. 3 shows the SEM/EDX images of the 50Si/GXGO composite (with the highest proportion of nSi) as a representative example of the series. Both the interconnected nodular structure of GXGO carbon matrix and the spherical silicon nanoparticles are visible and there is uniform contact between them. The nSi is composed of particles of about 50 nm in diameter. Moreover, a homogeneous distribution of the two materials is achieved, where GXGO is uniformly covered by nSi particles. No evidence of agglomerates of either nSi or GXGO was detected. This is largely due to the procedure used in the preparation of the composite, which produces a well-dispersed mixture of the two components without the need for additional milling steps that might modify the morphology of the material. This good dispersion also influences the electrochemical behavior of the material since it facilitates the accommodation role of the carbon matrix during the cycling processes and further leads to a more stable electrode in the long-term.

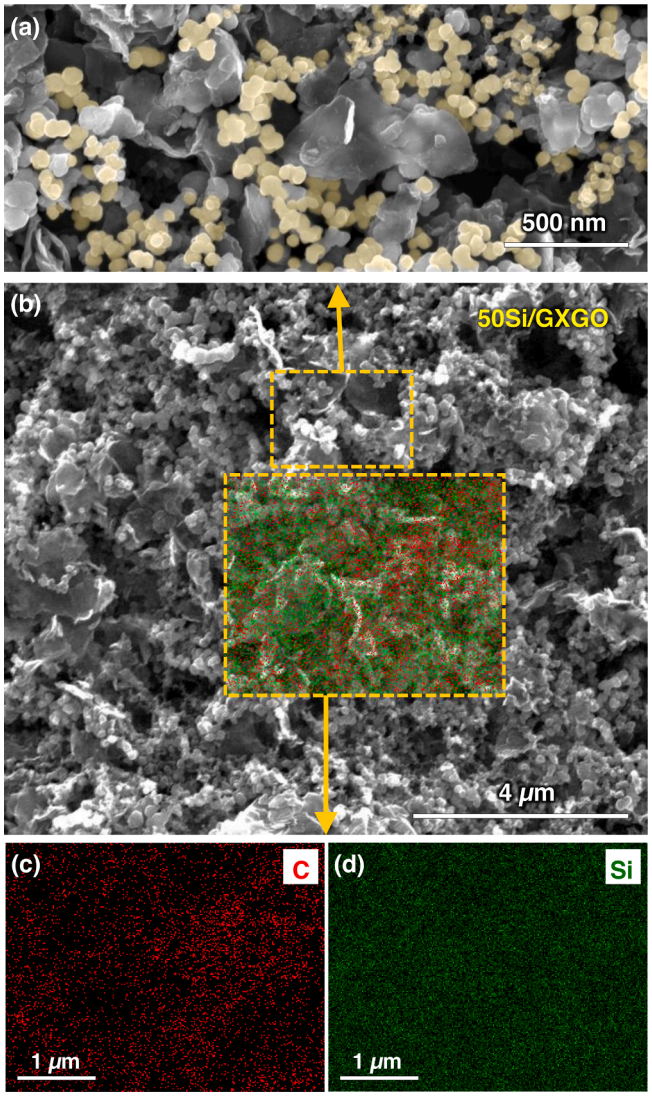

Fig. 3. SEM/EDX images of 50Si/GXGO composite.

3.3. Electrochemical performance as anodes of Si/GXGO composites

3.3.1. Influence of voltage range and electric current density of cycling

Fig. 4a shows the plots of specific capacity versus cycle number from galvanostatic cycling at a current density of 1000 mA g^{-1} of the electrodes containing nanosilicon, GXGO carbon matrix, and 20Si/GXGO composite as active materials. An overview of this data confirms that combining nSi and GXGO substantially improves the nano-silicon

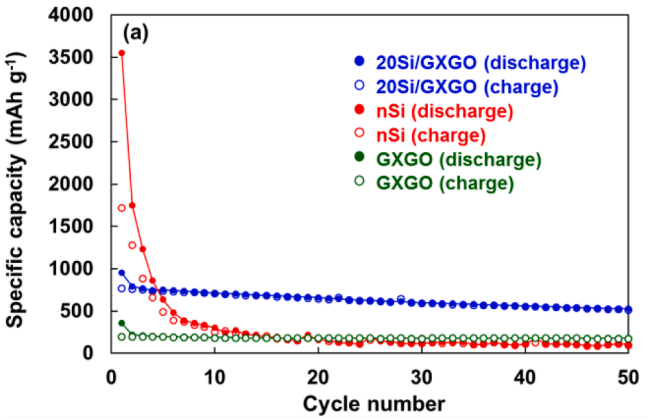

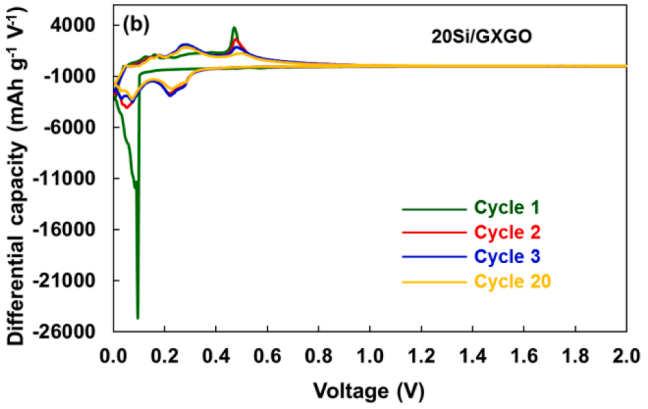

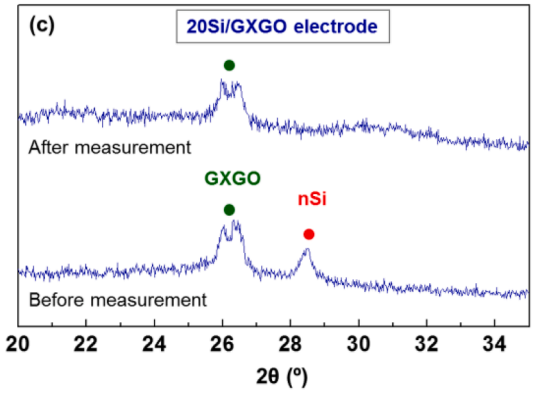

Fig. 4. (a) Specific discharge/charge capacity against cycle number plots from galvanostatic cycling at 1000 mA g^{-1} of nSi, GXGO, and 20Si/GXGO electrodes, in the 2.1–0.003 V voltage range, (b) Differential discharge/charge capacity against potential from galvanostatic cycling at 1000 mA g^{-1} of 20Si/GXGO electrode for 1st, 2nd, 3nd and 20th cycles, in the 2.1–0.003 V voltage range, and (c) XRD patterns of 20Si/GXGO electrode before and after electrochemical measurements (200 cycles).

electrode performance in terms of capacity and stability. Thus, a discharge capacity of 525 mAh g^{-1} (referring to the mass of the active composite material) with a coulombic efficiency of 99% after 50 discharge/charge cycles was calculated for the 20Si/GXGO electrode compared to only 101 mAh g^{-1} for the nSi electrode, whereas the former's capacity retention during cycling is much higher, i.e. 67% of the discharge capacity between cycles 2 and 50 for 20Si/GXGO versus 7% in the same interval for nSi. In addition, the loss of capacity during the first cycle due to the formation of the SEI layer (% irreversible capacity = $[C_{disc}$ (1st cycle) – C_{charge} (1st cycle)] $[C_{disc}$ (1st cycle)]$^{-1}$ x 100) of 20Si/GXGO is much lower (19% vs. 52% for nSi). To gain further insight into the interaction of Li^+ ions with the 20Si/GXGO active composite during the electrochemical process, the differential discharge/charge capacities against voltage plots for the 1st, 2nd, 3rd and 20th cycles in Fig. 4b were examined. The voltage drops quickly to ~ 0.1 V in the first discharge. At this potential, a broad band is observed, which is associated with the initial lithiation of the crystalline silicon (c-Si) to form an amorphous undefined a-Li_xSi alloy. At room temperature, the formation of the richest $Li_{15}Si_4$ phase, which according to Obrovac et al. [45] occurs only when all the crystalline silicon is lithiated at potentials below 50 mV, may lead to discharge capacities up to 3579 mAh g^{-1} as can be seen in Fig. 4a for the nSi electrode. In the subsequent charge there is a well-defined peak at ~ 0.47 V, which has been assigned to the de-lithiation of this alloy to produce amorphous silicon (a-Si). The lithiation (discharge) of the a-Si in the second cycle occurs in two steps, thus leading to two bands with maxima at ~ 0.23 and 0.05 V. As expected, the corresponding de-lithiation curve also shows two bands at approximately 0.28 and 0.47 V. In subsequent cycles, the two peaks from the de-lithiation of the a-Li_xSi alloy and those corresponding to its formation are also detected at the same potentials but lower intensity (Fig. 4b). Furthermore, there is a very small peak at < 0.04 V, which corresponds to the formation of the above mentioned $Li_{15}Si_4$ phase [44]. No additional discharge/charge peaks are observed at potentials higher than 0.9 V. These results agree with the observations from Obrovac et al. [45] and Li et al. [46] for the lithiation/de-lithiation mechanism of silicon electrodes. They are also confirmed by XRD data (Fig. 4c). Thus, the c-Si reflexion of the 20Si/GXGO electrode is clearly observed before the electrochemical measurements. However, this peak disappears completely after the discharge/charge cycles due to the formation of amorphous Li_xSi alloys, indicating that all the silicon contained in the electrode has been lithiated.

In addition to the use of the carbon matrix to accommodate the volume changes associated with the lithiation/de-lithiation process of the silicon, which significantly improved electrode performance (Fig. 4a), Obrovac et al. reported that the formation of a stable microstructure of a central crystalline Si that remains intact and a crust of amorphous Si in charge of the housing of the Li^+ ions could allow for greater control of these volume changes, thus better preventing electrode damage [45]. To reach this goal, the Li^+ ions' access to the silicon electrode during the first cycle should be limited by increasing the low cut-off voltage (LCOV) of cycling, so that c-Si lithiation will not be complete, but should be sufficient to obtain a significant initial capacity value. Therefore, it is necessary to determine the most suitable voltage range of cycling to optimize electrode performance. With this aim, the 20Si/GXGO electrode was subjected to galvanostatic cycling at a current density of 1000 mA g^{-1} for 200 cycles between 0.9 or 2.1 V and LCOV ranging from 3 to 80 mV. The galvanostatic plots (specific capacity against cycle number) are presented in Fig. 5a. In line with the aforementioned study by Obrovac et al. [45], the increase of the LCOV improves the capacity retention of 20Si/GXGO electrode during cycling. Thus, retention values regarding discharged capacity between cycles 2 and 200 of 44% and 80% were determined for LCOVs of 3 and 10 mV, respectively. This improvement goes in parallel with a reduction of the capacity during the first cycles due to limiting access of the Li^+ ions to the electrode, which will obviously determine its capacity at the end of cycling. Even so, a discharge capacity of 538 mAh g^{-1} with a coulombic

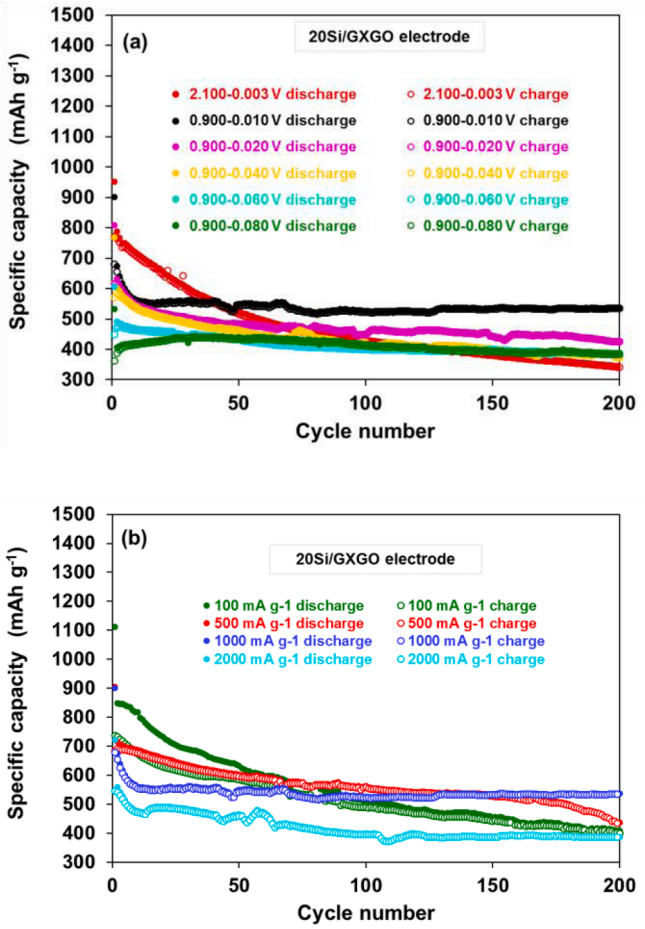

Fig. 5. (a) Specific discharge/charge capacity against cycle number plots from the galvanostatic cycling at 1000 mA g^{-1} of 20Si/GXGO electrode for 200 cycles between 0.9 or 2.1 V and low cut-off voltage ranging from 3 to 80 mV and (b) Specific discharge/charge capacity against cycle number plots from the galvanostatic cycling at 100, 500, 1000 and 2000 mA g^{-1} of 20Si/GXGO electrode for 200 cycles in the 0.9–0.010 V voltage range.

efficiency of 99.5% was obtained at a LCOV of 10 mV after 200 cycles in contrast to a value of 345 mAh g^{-1} at the initial LCOV of 3 mV. A subsequent increase of the LOCV up to 80 mV causes an improvement of the capacity retention during cycling (up to 95%), but leads to lower capacity (388 mAh g^{-1} after 200 cycles). As regards the electrode irreversible capacity in the first cycle, values of about 24% were determined for all of the LCOVs. In summary, it appears that at an LCOV of 10 mV it is possible to control the continuous microstructural changes of the silicon and therefore to restrict the volume changes in the electrode during the lithiation/de-lithiation process.

Fig. 5b shows the specific capacity versus cycle number plots obtained in prolonged galvanostatic cycling (200 cycles) of the 20Si/GXGO anode (versus metallic lithium) at current densities of 100, 500, 1000 and 2000 mA g^{-1} in the optimal voltage range of 0.9–0.010 V. As expected, an increase in the current density from 1000 to 2000 mA g^{-1} leads to a decrease in electrode capacity; even so, a final discharge capacity of 387 mAh g^{-1} with a coulombic efficiency of basically 100% was reached. At current densities lower than 1000 mA g^{-1}, such as 100 and 500 mA g^{-1}, the initial anode capacity increases significantly. However, under these lower currents, there is continuous anode capacity fading during cycling. For comparison, a capacity retention between cycles 2 and 200 of ~ 60% was calculated for the 20Si/GXGO electrode at 500 mA g^{-1} against 80% at 1000 mA g^{-1}. This effect is much more evident for the lowest current of 100 mA g^{-1} at which the discharge capacity retention in this cycling interval was only ~ 48%, in

such a way that, at the end of cycling, the anode capacity is similar to that obtained at the highest current of 2000 mA g^{-1}. At lower current densities, the time at which the electrode is in contact with the Li^+ ions increases, thus promoting the access of more ions to the electrode, which could progressively damage it by destroying the stable microstructure of a central crystalline Si [45]. Furthermore, at 100 mA g^{-1} the coulombic efficiency decreases substantially (charge time is longer than discharge time), particularly during the first 100 cycles with values below 90%. This may be due to electrolyte decomposition as a consequence of continuous formation of the SEI.

3.3.2. *Influence of the proportion of nSi in the Si/GXGO composite*

The influence of the proportion of nano-silicon on the electrochemical performance of YSi/GXGO composites as anodes was also investigated. To this end, GXGO-based composites containing different proportions of nSi (20, 30, 40 and 50 wt.%) were prepared. Fig. 6 shows the plots of these anodes' specific capacity versus cycle number obtained in galvanostatic cycling at the optimal current density of 1000 mA g^{-1} and voltage range of 0.9–0.010 V. For comparison, cycling results of electrodes based on the GXGO material, a commercial graphite (SG), and a commercial Si/C composite (carbon coated silicon) under the same experimental conditions are provided. The latter two materials were selected as references since they are both commercialized for anode materials of lithium-ion batteries. First of all, the combination of silicon at any proportion with the GXGO carbon matrix notably improves the performance of GXGO, SG and even Si/C electrodes. In fact, the capacity provided by the commercial Si/C composite are comparable to that of GXGO carbon material and it is even lower than that of graphite in these specific experimental conditions. This may be due to the fact that (i) the Li^+ ions do not reach the silicon cores of the composite and therefore the carbon material is the only active material, or (ii) the low amount of silicon in the composite (1.92 wt.%) is not enough to improve the capacity (at least to the order of that determined for graphite electrodes in LIBs).

In contrast, with the YSi/GXGO electrodes, good dispersion of nSi in the composite and the high pore size of the GXGO matrix allow Li^+ ions to diffuse into the electrode and makes it easier for them to reach the silicon nanoparticles, which improves the performance of the LIBs. Moreover, the scope of this improvement depends on the proportion of Si by weight in the active electrode composite. After 200 cycles, a discharge capacity of 538 mAh g^{-1} is obtained for the 20Si/GXGO electrode compared to 321 and 145 mAh g^{-1} for graphite and GXGO electrodes, respectively. The coulombic efficiency is basically 100% in all cases. Increasing the proportion of nSi further, up to 30 wt.%, leads to much higher capacity values with a final discharge capacity of 917 mAh g^{-1} and in addition the electrode remains stable during cycling, thus confirming the capacity of the GXGO carbon matrix to accommodate the volume changes associated with the lithiation/de-lithiation process in the 30Si/GXGO electrode. On the contrary, larger proportions of nSi in the active composite (40 or 50 wt.%) allow the insertion of many more Li^+ ions in the first cycles, as corroborated by the values of the discharge capacity, i.e. 1489 and 1240 mAh g^{-1} for 50Si/GXGO and 40Si/GXGO electrodes, respectively, in the 10th cycle versus 1091 mAh g^{-1} for 30Si/GXGO. This leads to a progressive loss of capacity during cycling due to electrode damage because the structure collapses [44]. For example, between cycles 2 and 50, the discharge capacity provided by 50Si/GXGO decreased by around 50% compared to 14% for 30Si/GXGO. Therefore, a proportion of 30 wt.% of nSi in the active composite seems to be optimum, since it is a compromise between a suitable specific capacity, which is about three times higher than that of the commercially available graphite electrode for LIBs, and good capacity retention (77% between cycles 2 and 200). For comparison, capacity values in the range of 1100–800 mAh g^{-1} were reported for a granadilla-like Si/C composite (30 wt.% Si) [41] and for a graphene bubble film Si/C composite (58 wt.% Si) [36], respectively, after prolonged galvanostatic cycling but at lower electrical current densities (250–100 mA g^{-1}). However, these composites were prepared by more complex procedures which, among others, included templating, CVD and chemical functionalization.

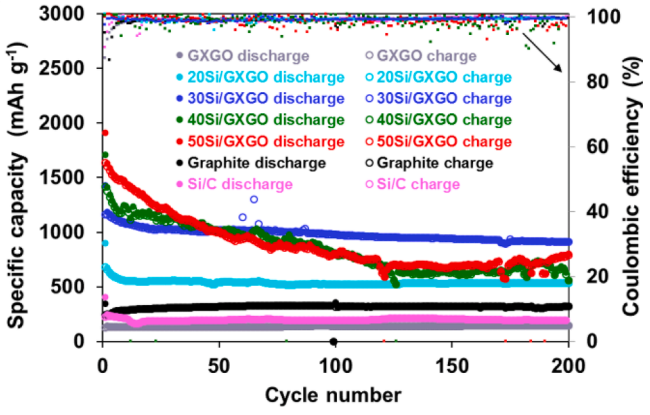

Fig. 6. Specific discharge/charge capacity and coulombic efficiency against cycle number plots from galvanostatic cycling of YSi/GXGO ($Y = 20$, 30, 40 and 50) electrodes in the 0.9 - 0.010 V voltage range at a current density of 1000 mA g^{-1}.

4. Conclusions

Silicon-carbon composite materials were prepared to be used as anodes in lithium-ion batteries by following a cost-effective, simple, easily-scalable procedure. In order to do that, a graphitic carbon xerogel matrix was synthetized by a microwave assisted approach and nanocrystalline silicon was incorporated by simply dispersing the two materials in 2-isopropanol. The GXGO carbon matrix presented a pore size of 275 nm and a homogenous distribution of silicon into this matrix was obtained, resulting in an electrode with an excellent microstructure. Various electrochemical conditions were evaluated to determine the most suitable. The optimal potential range and current density were 0.9–0.010 V and 1000 mA g^{-1}, respectively. The anodic behavior of Si/GXGO composites with different proportions of nSi was also studied. The composite with 30 wt.% of nSi showed the best performance, with a specific discharge capacity value as high as 917 mAh g^{-1} after 200 cycles at an electric current of 1000 mA g^{-1}, a coulombic efficiency of 100% and good capacity retention. The reason for this high performance was a combination of the following factors: (i) homogeneous distribution of silicon nanoparticles in the GXGO carbon matrix which allows intimate Si/GXGO contact; and (ii) a porous carbon network of the GXGO material that is able to accommodate the huge volume changes associated with the silicon lithiation/de-lithiation process, which may be restricted under suitable cycling conditions related to potential limitations in order to control continuous microstructural changes in the silicon, thus preserving electrode integrity and avoiding capacity fading. The Si/GXGO composites investigated in this study demonstrate great potential for use as anode material in next-generation LIBs.

CRediT authorship contribution statement

Lucía dos Santos-Gómez: Conceptualization, Methodology, Investigation, Formal analysis, Writing – original draft, Writing – review & editing. **Nuria Cuesta:** Conceptualization, Methodology, Investigation, Writing – review & editing. **Ignacio Cameán:** Conceptualization, Methodology, Investigation, Formal analysis, Writing – original draft, Writing – review & editing. **S. García-Granda:** Project administration, Writing – review & editing. **Ana B. García:** Conceptualization, Investigation, Formal analysis, Validation, Project administration, Writing – original draft, Writing – review & editing. **Ana Arenillas:** Conceptualization, Investigation, Formal analysis, Validation, Project

administration, Writing – review & editing.

Declaration of Competing Interest

The authors declare that they have no known competing financial interests or personal relationships that could have appeared to influence the work reported in this paper.

Data availability

Data will be made available on request.

Acknowledgments

This research was supported by MCIN/AEI/10.13039/501100011033 and "European Union NextGenerationEU/PRTR" (Project ID2020–113001RB-I00) and Asturian Regional Government (GRUPIN2021 IDI/2021/000031). Lucía dos Santos-Gómez thanks the Ministerio de Ciencia, Innovación y Universidades for her Juan de la Cierva Incorporación grant (IJC2020–044746-I). Ignacio Cameán acknowledges the funding from Fundación General CSIC (Programa ComFuturo, II Edition).

References

[1] Z.P. Cano, D. Banham, S. Ye, A. Hintennach, J. Lu, M. Fowler, Z. Chen, Batteries and fuel cells for emerging electric vehicle markets, Nat. Energy 3 (2018) 279–289.
[2] B. Scrosati, J. Hassoun, Y.K. Sun, Lithium-ion batteries. A look into the future, Energy Environ. Sci. 4 (2011) 3287–3295.
[3] M. Armand, J.M. Tarascon, Building better batteries, Nature 451 (2008) 652–657.
[4] N. Cuesta, I. Cameán, A. Ramos, A.B. García, Graphitized biogas-derived carbon nanofibers as anodes for lithium-ion batteries, Electrochim. Acta 222 (2016) 264–270.
[5] G. Wang, M. Yu, X. Feng, Carbon materials for ion-intercalation involved rechargeable battery technologies, Chem. Soc. Rev. 50 (2021) 2388–2443.
[6] L. Li, D. Zhang, J. Deng, Y. Gou, J. Fang, H. Cui, et al., Carbon-based materials for fast charging lithium-ion batteries, Carbon 183 (2021) 721–734.
[7] M. Kakunuri, C.S. Sharma, Resorcinol-formaldehyde derived carbon xerogels: a promising anode material for lithium-ion battery, J. Mater. Res. 33 (2018) 1074–1087.
[8] M.L.C. Piedboeuf, A.F. Léonard, F.L. Deschamps, N. Job, Carbon xerogels as model materials: toward a relationship between pore texture and electrochemical behavior as anodes for lithium-ion batteries, J. Mater. Sci. 51 (2016) 4358–4370.
[9] M.L.C. Piedboeuf, A.F. Léonard, G. Reichenauer, C. Balzer, N. Job, How do the micropores of carbon xerogels influence their electrochemical behavior as anodes for lithium-ion batteries? Micropor. Mesopor. Mat. 275 (2019) 278–287.
[10] N. Rey-Raap, J. Angel Menéndez, A. Arenillas, Simultaneous adjustment of the main chemical variables to fine-tune the porosity of carbon xerogels, Carbon 78 (2014) 490–499.
[11] N. Rey-Raap, J.A. Menéndez, A. Arenillas, Optimization of the process variables in the microwave-induced synthesis of carbon xerogels, J. Sol-Gel Sci. Technol. 69 (2014) 488–497.
[12] I.D. Alonso-Buenaposada, N. Rey-Raap, E.G. Calvo, J. Angel Menéndez, A. Arenillas, Effect of methanol content in commercial formaldehyde solutions on the porosity of RF carbon xerogels, J. Non-Cryst. Solids 426 (2015) 13–18.
[13] F. Meng, X. Zhang, B. Xu, S. Yue, H. Guo, Y. Luo, Alkali-treated graphene oxide as a solid base catalyst: synthesis and electrochemical capacitance of graphene/carbon composite aerogels, J. Mater. Chem. 21 (2011) 18537–18539.
[14] Z.M. Marković, B.M. Babić, M.D. Dramićanin, I.D. Holclajtner Antunović, V. B. Pavlović, D.B. Peruško, B.M. Todorović Marković, Preparation of highly conductive carbon cryogel based on pristine graphene, Synth. Met. 162 (2012) 743–747.
[15] Z. Ling, G. Wang, Q. Dong, B. Qian, M. Zhang, C. Li, J. Qiu, An ionic liquid template approach to graphene–carbon xerogel composites for supercapacitors with enhanced performance, J. Mater. Chem. A 2 (2014) 14329–14333.
[16] M. Canal-Rodríguez, J.A. Menéndez, M.A. Montes-Morán, I. Martín-Gullón, J. B. Parra, A. Arenillas, The role of conductive additives on the performance of hybrid carbon xerogels as electrodes in aqueous supercapacitors, Electrochim. Acta 295 (2019) 693–702.
[17] M. Canal-Rodríguez, A. Arenillas, J.A. Menéndez, D. Beneroso, N. Rey-Raap, Carbon xerogels graphitized by microwave heating as anode materials in lithium-ion batteries, Carbon 137 (2018) 384–394.
[18] M. Canal-Rodríguez, A. Arenillas, S.F. Villanueva, M.A. Montes-Morán, J. A. Menénedez, Graphitized carbon xerogels for lithium-ion batteries, Materials 13 (2020) 119.
[19] M.M. Gaikwad, M. Kakunuri, C.S. Sharma, Enhanced catalytic graphitization of resorcinol formaldehyde derived carbon xerogel to improve its anodic performance for lithium ion battery, Mater. Today Commun. 20 (2019), 100569.
[20] X. Zuo, J. Zhu, P. Müller-Buschbaum, Y.J. Cheng, Silicon based lithium-ion battery anodes: a chronicle perspective review, Nano Energy 31 (2017) 113–143.
[21] M.L. Terranova, S. Orlanducci, E. Tamburri, V. Guglielmotti, M. Rossi, Si/C hybrid nanostructures for Li-ion anodes: an overview, J. Power Sources 246 (2014) 167–177.
[22] P. Li, G. Zhao, X. Zheng, X. Xu, C. Yao, W. Sun, S.X. Dou, Recent progress on silicon-based anode materials for practical lithium-ion battery applications, Energy Storage Mater. 15 (2018) 422–446.
[23] B.A. Boukamp, G.C. Lesh, R.A. Huggins, All-solid lithium electrodes with mixed-conductor matrix, J. Electrochem. Soc. 128 (1981) 725–729.
[24] Z. Lu, T. Wong, T.W. Ng, C. Wang, Facile synthesis of carbon decorated silicon nanotube arrays as anode material for high-performance lithium-ion batteries, RSC Adv. 4 (2014) 2440–2446.
[25] Y. Fan, Q. Zhang, Q. Xiao, X. Wang, K. Huang, High performance lithium ion battery anodes based on carbon nanotube–silicon core–shell nanowires with controlled morphology, Carbon 59 (2013) 264–269.
[26] J. Miao, C.V. Thompson, Kinetic study of the initial lithiation of amorphous silicon thin film anodes, J. Electrochem. Soc. 165 (2018) A650–A656.
[27] A. Mukanova, A. Nurpeissova, A. Urazbayev, S.S. Kim, M. Myronov, Z. Bakenov, Silicon thin film on graphene coated nickel foam as an anode for Li-ion batteries, Electrochim. Acta 258 (2017) 800–806.
[28] J.R. Szczech, S. Jin, Nanostructured silicon for high capacity lithium battery anodes, Energy Environ. Sci. 4 (2011) 56–72.
[29] M.A. Rahman, G. Song, A.I. Bhatt, Y.C. Wong, C. Wen, Nanostructured silicon anodes for high-performance lithium-ion batteries, Adv. Funct. Mater. 26 (2016) 647–678.
[30] J. Shim, R. Kostecki, T. Richardson, X. Song, K.A. Striebel, Electrochemical analysis for cycle performance and capacity fading of a lithium-ion battery cycled at elevated temperature, J. Power Sources 112 (2002) 222–230.
[31] C. Erk, T. Brezesinski, H. Sommer, R. Schneider, J. Janek, Toward silicon anodes for next-generation lithium ion batteries: a comparative performance study of various polymer binders and silicon nanopowders, ACS Appl. Mater. Interfaces 5 (2013) 7299–7307.
[32] A. Uctepe, E. Demir, B. Tekin, B. Dursun, O. Ozturk, O. Sel, R. Demir-Cakan, Prompt microwave-assisted synthesis of carbon coated Si nanocomposites as anode for lithium-ion batteries, Solid State Ion 354 (2020), 115409.
[33] M. Cabello, E. Gucciardi, A. Herrán, D. Carriazo, A. Villaverde, T. Rojo, Towards a high-power Si@graphite anode for lithium ion batteries through a wet ball milling process, Molecules 25 (2020) 2494.
[34] I. Cameán, N. Cuesta, A. Ramos, A.B. García, Silicon/biogas-derived carbon nanofibers composites for anodes of lithium-ion batteries, *C* J. Carbon Res. 6 (2020) 25.
[35] H.K. Han, C. Loka, Y.M. Yang, J.H. Kim, S.W. Moon, J.S. Cho, K.S. Lee, High capacity retention Si/silicide nanocomposite anode materials fabricated by high-energy mechanical milling for lithium-ion rechargeable batteries, J. Power Sources 281 (2015) 293–300.
[36] X. Liu, C. Shen, L. Lu, G. Liu, Y. Jiang, Y. Gao, W. Li, B. Zhao, J. Zhang, Graphene bubble film encasulapted Si@C hollow spheres as a durable anode material for lithiun storage, Electrochim. Acta 361 (2020), 137074.
[37] Y. An, H. Fei, G. Zeng, L. Ci, S. Xiong, J. Feng, Y. Qian, Green, scalable, and controllable fabrication of nanoporous silicon from commercial alloy precursors for high-energy lithium-ion batteries, ACS Nano 12 (2018) 4993–5002.
[38] M. Wu, J.E. Sabisch, X. Song, A.M. Minor, V.S. Battaglia, G. Liu, *In situ* formed Si nanoparticle network with micron-sized Si particles for lithium-ion battery anodes, Nano Lett. 13 (2013) 5397–5402.
[39] N.S. Choi, K.H. Yew, K.Y. Lee, M. Sung, H. Kim, S.S. Kim, Effect of fluoroethylene carbonate additive on interfacial properties of silicon thin-film electrode, J. Power Sources 161 (2006) 1254–1259.
[40] D. Bresser, D. Buchholz, A. Moretti, A. Varzi, S. Passerini, Alternative binders for sustainable electrochemical energy storage – the transition to aqueous electrode processing and bio-derived polymers, Energy Environ. Sci. 11 (2018) 3096–3127.
[41] Q. Shi, J. Zhou, S. Ullah, X. Yang, K. Tokarska, B. Trzebicka, H.Q. Ta, M. H. Rümmeli, A review of recent developments in Si/C composite materials for Li-ion batteries, Energy Storage Mater. 34 (2021) 735–754.
[42] E. Calvo, E. Juárez-Pérez, J. Menéndez, A. Arenillas, Fast microwave-assisted synthesis of tailored mesoporous carbon xerogels, J. Colloid Interface Sci. 357 (2011) 541–547.
[43] M. Canal-Rodríguez, A. Arenillas, N. Rey-Raap, G. Ramos-Fernández, I. Martín-Gullón, J.A. Menéndez, Graphene-doped carbon xerogel combining high electrical conductivity and surface area for optimized aqueous supercapacitors, Carbon 118 (2017) 291–298.
[44] B. Amelo, 'Pert HighScore Plus, version 3.0 e, The Netherlands (2012).
[45] M. Obrovac, L. Krause, Reversible cycling of crystalline silicon powder, J. Electrochem. Soc. 154 (2006) A103.
[46] J. Li, J. Dahn, An *in situ* X-ray diffraction study of the reaction of Li with crystalline Si, J. Electrochem. Soc. 154 (2007) A156.